Available online at www.sciencedirect.com
SCIENCE DIRECT
Acta Materialia 54 (2006) 2419–2429
Acta MATERIALIA
www.actamat-journals.com

Martensitic transformation, shape memory effect and superelasticity of Ti–Nb binary alloys

H.Y. Kim [a,*], Y. Ikehara [a], J.I. Kim [a], H. Hosoda [b], S. Miyazaki [a,*]

[a] *Institute of Materials Science, University of Tsukuba, Tsukuba, Ibaraki 305 8573, Japan*
[b] *Precision and Intelligence Laboratory, Tokyo Institute of Technology, Yokohama 226 8503, Japan*

Received 20 December 2005; accepted 20 January 2006
Available online 23 March 2006

Abstract

Shape memory and superelastic properties associated with the martensitic transformation from β to α″ martensite were investigated in Ti–(15–35) at.% Nb alloys. The transformation strain and transformation temperature linearly decreased with increasing Nb content. The low critical stress for slip deformation resulted in only a small superelastic strain in solution-treated Ti–Nb binary alloys. Fine and dense ω precipitates formed during aging in the temperature range between 573 and 673 K were effective in increasing the critical stress for slip deformation in a Ti–26 at.% Nb alloy. An intermediate-temperature annealing at 873 K for 600 s without solution treatment was also effective in increasing the critical stress for slip deformation due to the fine subgrain structure. The higher critical stress for slip deformation resulted in a larger recovery strain and stable superelasticity. Excellent superelasticity was achieved by annealing at 873 K for 600 s followed by aging at 573 K due to the combined effect of work hardening and age hardening.

Keywords: Shape memory alloys; Superelasticity; Biomaterials; Titanium alloys; Precipitation

1. Introduction

Ti–Ni shape memory alloys have been successfully applied as biomedical materials, such as orthodontic arch wires, bone plates and stents, owing to their superior shape memory properties, superelasticity and corrosion resistance. Recently, the issues of the hypersensitivity and toxicity of Ni have stimulated the development of Ni-free shape memory alloys. Continuing research and developmental efforts have shown that β-type Ti-based alloys are promising materials for biomedical shape memory and superelastic alloys [1–7].

Ti-based alloys have been widely used as biomaterials due to their high corrosion resistance, good biocompatibility, high strength and low elastic modulus. The β-type Ti alloys also exhibit a martensitic transformation from β (disordered body-centered cubic) to orthorhombic (α″) martensite above a critical alloying content. It was first reported by Baker [8] that a change of α″ to β resulted in a shape memory effect in Ti–35 wt.% Nb (Ti–21.7 at.% Nb) alloy. Although he reported that aging of short durations at 573–773 K improved shape recovery due to the precipitation of ω phase, he did not demonstrate superelasticity. Furthermore, microstrcutural observation and quantitative analysis of the relationship between shape memory properties and ω phase have not been conducted. The shape memory effect has also been observed in Ti–10V–2Fe–3Al (wt.%) [1], Ti–15.4V–4Al (wt.%) [9] and Ti–Mo–Al alloys [10] with recoverable strains in the range 3.0–4.0%. It is noted that these alloys do not exhibit superelasticity at room temperature. Recently it has been reported that superelasticity can be obtained in Ti–Nb- and Ti–Mo-based multinary alloys such as β-Cez (Ti–4Mo–4.4Zr–4.9Al–2Sn–2Cr–1Fe (wt.%)) [2], Ti–Nb–Sn [3], Ti–(8–10)Mo–4Nb–2V–3Al (wt.%) [5], Ti–Nb–Al [6], Ti–Mo–Ga [7], Ti–Nb–Zr [11], Ti–Nb–O [12] and Ti–Nb–Ta [13] alloys.

* Corresponding authors. Tel./fax: +81 298 53 5283.
E-mail addresses: heeykim@ims.tsukuba.ac.jp (H.Y. Kim), miyazaki@ims.tsukuba.ac.jp (S. Miyazaki).

1359-6454/$30.00
doi:10.1016/j.actamat.2006.01.019

Superelasticity has also been observed in Ti–Nb binary alloys at room temperature, although the recovery strain is small due to the low critical stress for slip deformation [14]. In order to improve the superelasticity of binary Ti–Nb alloys, it is necessary to increase the critical stress for slip deformation. Two different approaches are suggested in this study. One is an aging treatment after the solution treatment, using the precipitation hardening effect due to the fine ω phase. The ω phase in Ti-based alloys has been studied extensively because of its deleterious effects on mechanical properties. The ω phase is a metastable phase existing in Ti- and Zr-based alloys containing β-stabilizing elements. The ω phase can even be formed by quenching from a high temperature, when it is known as athermal ω phase. Another type of ω phase can also be formed by aging at a low or intermediate temperature, this being called thermal ω phase. It is generally acknowledged that the thermal ω phase leads to a severe loss of ductility and an increase in hardness. Although some reports have been published on the ω phase in Ti–Nb binary alloys, no detailed study has reported on the effect of ω phase on shape memory and superelastic properties. The other method suggested for increasing the critical stress for slip deformation in Ti–Nb binary alloys is intermediate-temperature annealing rather than solution treatment after cold rolling, making use of the work hardening effect.

The superelastic strain is determined by the lattice deformation creating a martensite lattice from a parent lattice. Therefore, it is very important to investigate the lattice constants of the parent and martensite phases in Ti–Nb-based alloys in order to develop superelastic alloys with a larger recovery strain. However, the reported lattice constants of the α″ martensite and β parent phases show a broad scatter [15–19].

In this study, the effect of Nb content on the transformation strain was investigated by measuring the lattice constants of the parent and martensite phases in Ti–(15–35) at.% Nb alloys. The effect of aging temperature and time on the formation of ω phase in a solution-treated Ti–26 at.% Nb alloy was investigated using transmission electron microscopy (TEM). The effect of ω phase on the mechanical properties and shape memory and superelastic behavior was investigated using tensile tests. The effect of intermediate-temperature annealing on the microstructure and superelastic behavior was also investigated.

2. Experimental

The Ti–(15–35) at.% Nb alloys were prepared using the Ar arc melting method. The ingots were sealed in a vacuum in a quartz tube and homogenized at 1273 K for 7.2 ks, 4and then cold-rolled with a reduction in thickness of 99%. Specimens for X-ray diffraction (XRD) measurements, mechanical tests and TEM observation were cut using an electro-discharge machine. The damaged surface was removed by mechanical polishing and chemical etching. The specimens were cleaned with ethanol, wrapped in Ti foils and encapsulated in quartz tubes under a 25 Torr partial pressure of high-purity Ar, and then solution treated at 1173 K for 1.8 ks. The specimens were quenched into water by breaking the quartz tubes. After the solution treatment, some specimens were aged at temperatures of between 473 and 873 K. Some cold-rolled specimens were annealed at 873 K for 0.6 ks without solution treatment, followed by aging at 573 K for 3.6 ks.

XRD measurements were conducted at room temperature with Cu Kα radiation. Tensile tests were carried out at a strain rate of $1.67 \times 10^{-4}\ s^{-1}$ at various temperatures. The gage length of specimens was 20 mm. Specimens for TEM observation were prepared by a conventional twin-jet polishing technique. TEM observations were conducted using a JEOL2010F instrument operated at 200 kV.

3. Results and discussion

3.1. Lattice constants of β and martensite phases in Ti–Nb alloys

A schematic of the crystal structures of the β austenite phase and α″ orthorhombic martensite phase is shown in Fig. 1. The lattice correspondence between β and α″ phases can be expressed as follows:

$$[100]_{\beta}–[100]_{\alpha''},\quad [010]_{\beta}–\frac{1}{2}[01\bar{1}]_{\alpha''},\quad [001]_{\beta}–\frac{1}{2}[011]_{\alpha''}$$

alternatively

$$[100]_{\alpha''}–[100]_{\beta},\quad [010]_{\alpha''}–[011]_{\beta},\quad [001]_{\alpha''}–[0\bar{1}1]_{\beta}$$

The lattice constants of the β and α″ phases were measured at room temperature in Ti–(15–35) at.% Nb alloys and they are plotted as a function of Nb content in Fig. 2. It is seen from Fig. 2(a) that the lattice constant a_0 of the β phase slightly increases by 0.013×10^{-3} nm/1 at.% Nb in the Ti–(22–35) at.% Nb alloys. The Nb content dependence of a', b' and c' of the α″ orthorhombic martensite phase

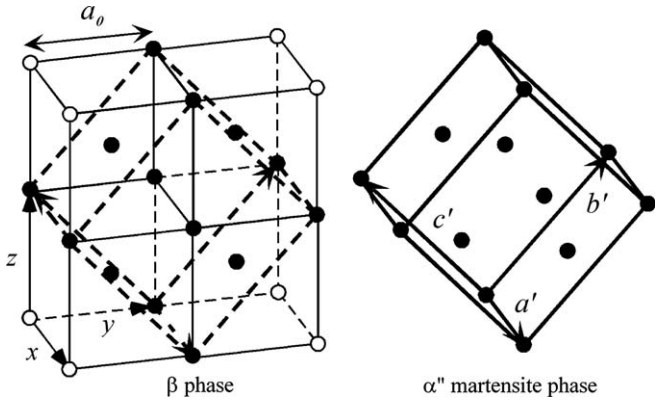

Fig. 1. A schematic illustration exhibiting lattice correspondence between β and α″ phases.

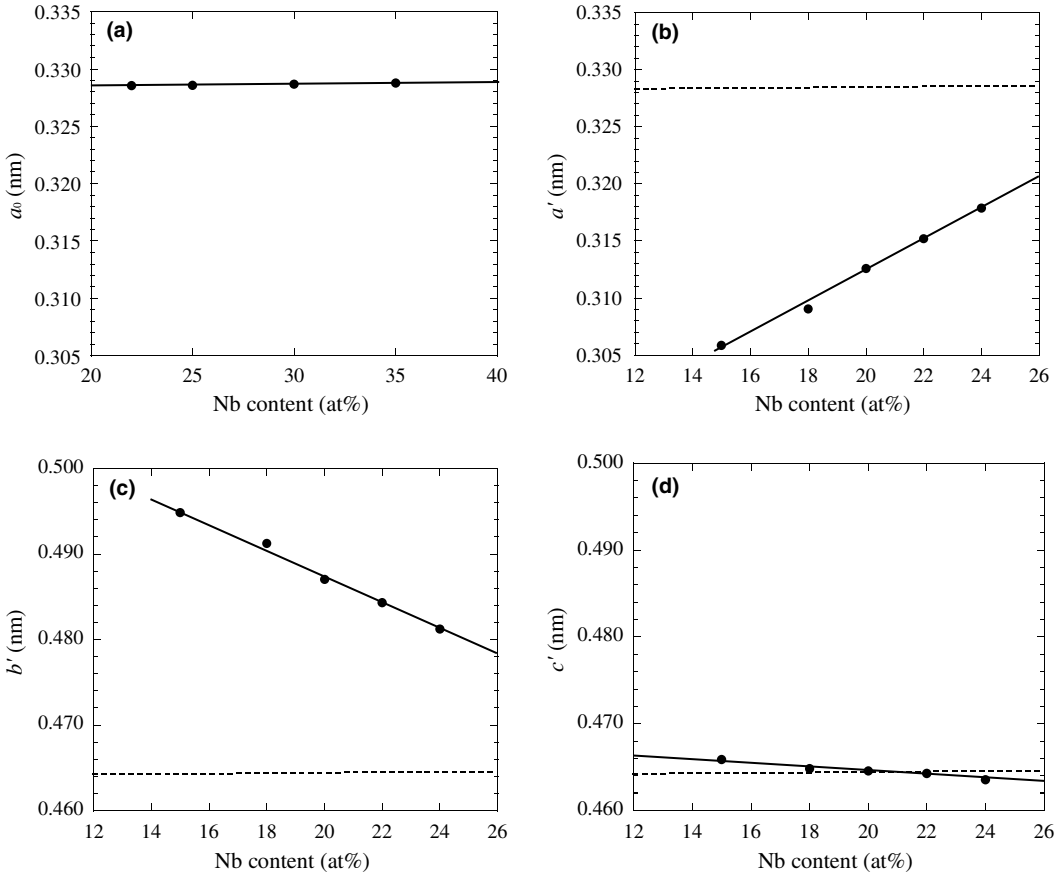

Fig. 2. Nb content dependence of the lattice constants of the β and α″ phases.

is shown in Fig. 2(b)–(d), respectively. The lattice constants of the α″ phase change linearly in the Ti–(15–24) at.% Nb alloys: a' increases by 1.364×10^{-3} nm and b' decreases by 1.546×10^{-3} nm with a 1 at.% increase of Nb. The change of c' is small compared with those of a' and b', i.e. -0.238×10^{-3} nm/1 at.% Nb.

The lattice deformation strains (η_1, η_2 and η_3) needed to form the α″ phase from the β phase along the three principal axes of $[1\,0\,0]_{\alpha''}$, $[0\,1\,0]_{\alpha''}$ and $[0\,0\,1]_{\alpha''}$ were calculated and they are plotted as a function of Nb content in Fig. 3 for the Ti–(15–24) at.% Nb alloys. The lattice constant of the β phase for the Ti–(15–20) at.% Nb alloys was determined by extrapolation using the linear dependence of lattice constant on Nb content as shown in Fig. 2. Fig. 3 reveals that two principal lattice strains (η_1 and η_2) of the martensitic transformation are approximately equal and opposite in sign, and their absolute values decrease with increasing Nb content for the Ti–(15–24) at.% Nb alloys. Lattice strain η_3 is small compared with η_1 and η_2, ranging from −0.24% to 0.30%.

The transformation strain due to the martensitic transformation from the β to α″ phase was calculated using the lattice constants of the parent β phase (a_0) and those of the orthorhombic α″ martensite phase (a', b', c'). The lattice distortion matrix **T** with respect to the coordinates of the parent β phase can be expressed as follows:

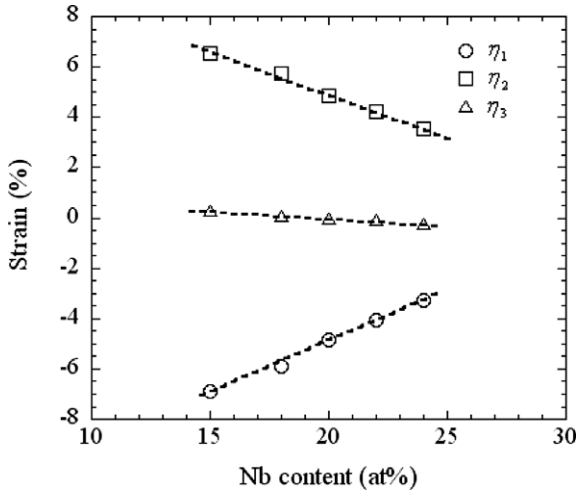

Fig. 3. Nb content dependence of the lattice deformation strains needed to form the α″ from the β phase along the three principal axes of the α″ phase.

$$\mathbf{T} = \begin{bmatrix} a'/a_0 & 0 & 0 \\ 0 & (b'+c')/2\sqrt{2}a_0 & (b'-c')/2\sqrt{2}a_0 \\ 0 & (b'-c')/2\sqrt{2}a_0 & (b'+c')/2\sqrt{2}a_0 \end{bmatrix}. \quad (1)$$

If we assume that a given vector **x** in the coordinates of the parent phase is transformed to **x**′ due to the martensitic

transformation, the maximum transformation strain ε_M^i along each orientation can be calculated as follows:

$$\varepsilon_M^i = \frac{|\mathbf{x}'| - |\mathbf{x}|}{|\mathbf{x}|}, \tag{2}$$

where $\mathbf{x}' = \mathbf{T}\mathbf{x}$. For example, the calculated result of the transformation strain ε_M^i for the Ti–22 at.% Nb alloy is shown in Fig. 4. ε_M^i is expressed by contour lines for each orientation in a [0 0 1]–[0 1 1]–[$\bar{1}$ 1 1] standard stereographic triangle. The maximum transformation strain of 4.2% was obtained along the [0 1 1] direction. The transformation strain decreases with changing direction from the [0 1 1] toward the [0 0 1] and [$\bar{1}$ 1 1] directions. The transformation strains along the [0 0 1] and [$\bar{1}$ 1 1] directions were calculated to be 2.1 and 1.5%, respectively. This indicates that the maximum transformation strain can be obtained when the loading axis is parallel to the [0 1 1] direction. The average transformation strain $\bar{\varepsilon}_M$ for a polycrystal with randomly distributed grains was estimated by a simple approximation of averaging ε_M^i for 36 representative orientations located in the [0 0 1]–[0 1 1]–[$\bar{1}$ 1 1] standard stereographic triangle. The maximum transformation strain, i.e. the transformation strain along the [0 1 1] direction, and the average transformation strain $\bar{\varepsilon}_M$ are plotted as a function of Nb content in Fig. 5(a). The maximum transformation strain $\varepsilon_M^{[0\,1\,1]}$ decreases with increasing Nb content and can be expressed by the following equation:

$$\varepsilon_M^{[0\,1\,1]}(\%) = 11.7 - 0.34 \times C_{Nb}(\text{at.}\%), \tag{3}$$

where C_{Nb} (at.%) is the Nb content. This means that a larger shape recovery strain can be obtained in an alloy with a lower Nb content. The martensitic transformation start temperature M_s also decreases with increasing Nb content as shown in Fig. 5(b) [8,14,20,21]. M_s decreases by 40 K with a 1 at.% increase of Nb content for Ti–(20–28) at.% Nb alloys. M_s becomes lower than room temperature when the Nb content increases more than 25.5 at.%.

Fig. 6 shows a series of stress–strain curves obtained at various temperatures for the Ti–(26–28) at.% Nb alloys after solution treatment at 1173 K for 1.8 ks. The tensile stress was applied until the strain reached about 2.5%, and then the stress was removed. After unloading, specimens that did not exhibit complete superelastic recovery were heated to about 500 K: broken lines with an arrow

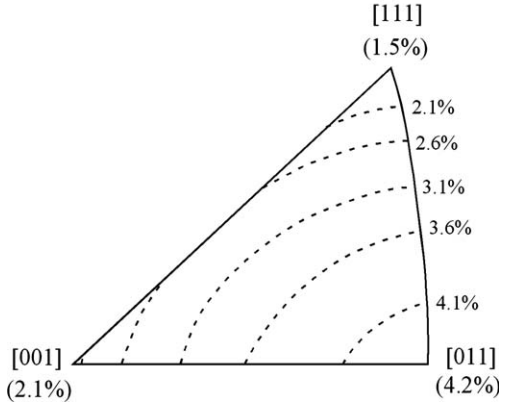

Fig. 4. Orientation dependence of the calculated transformation strain associated with the martensitic transformation from the β to α″ phase in the Ti–22 at.% Nb alloy.

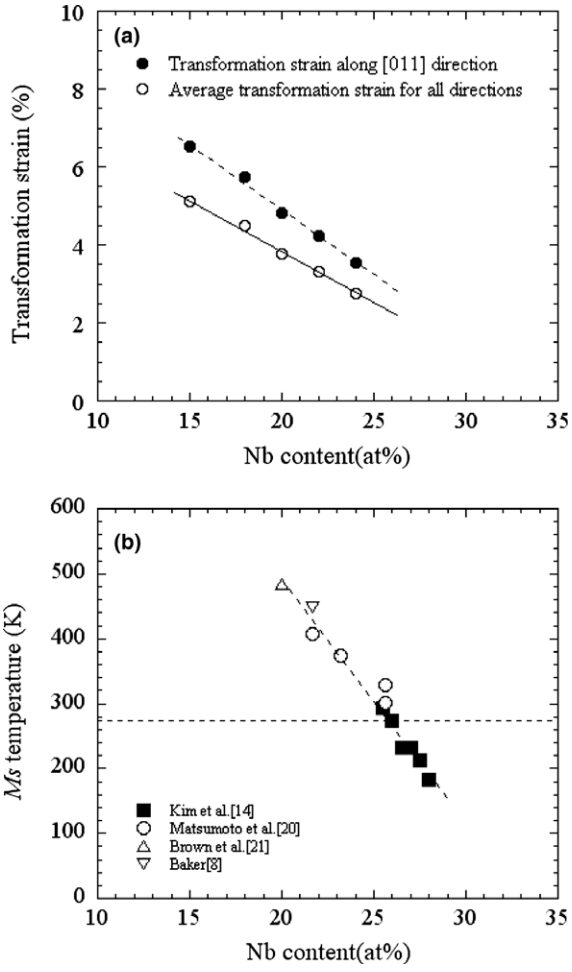

Fig. 5. Nb content dependence of the transformation strain (a) and martensitic transformation start temperature (b).

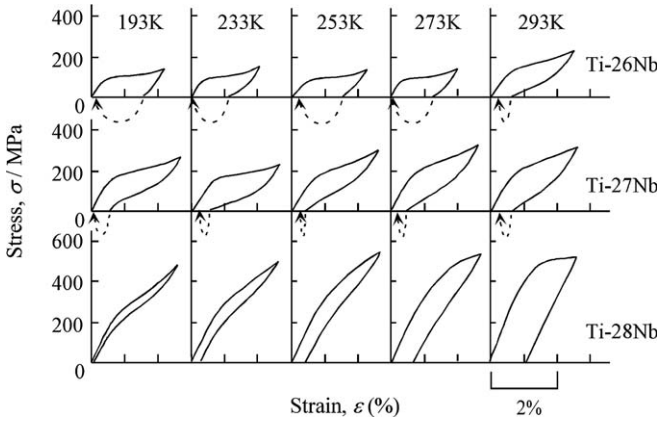

Fig. 6. Stress–strain curves obtained upon loading and unloading at various temperatures for the Ti–(26–28) at.% Nb alloys.

indicate shape recovery by heating. The shape memory effect was observed for the Ti–26 at.% Nb alloy deformed at temperatures between 193 and 273 K. The residual strain after unloading was completely recovered by heating to about 500 K. Superelastic behavior was observed at 293 K, although the shape recovery was incomplete. For the Ti–27 at.% Nb alloy, incomplete superelastic behavior was also observed at temperatures between 193 and 293 K. The residual strain was recovered by heating. This indicates that the finish temperature of the reverse transformation (A_f) is higher than 293 K for the Ti–27 at.% Nb alloy. The Ti–28 at.% Nb alloy exhibited excellent superelastic behavior at 193 K. The residual strain increased with increasing temperature. Shape recovery was hardly observed when the test temperature was higher than 273 K. The critical stress to induce the martensitic transformation increased with increasing temperature, while the critical stress for slip decreased with increasing temperature. Slip occurs if the critical stress level for slip becomes lower than the stress to induce the martensite. Thus, the strain by slip deformation increased with increasing temperature, causing the recoverable strain to decrease. As a result, it is concluded that the low critical stress for slip deformation caused the superelasticity not to reveal a large strain in the solution-treated binary Ti–Nb alloys.

3.2. Effect of aging treatment on tensile property and microstructure

Fig. 7 shows stress–strain curves of Ti–26 at.% Nb specimens aged at temperatures between 473 and 873 K for 3.6 ks after solution treatment. The stress–strain curve of a specimen solution treated at 1173 K for 1.8 ks is also shown for reference. All specimens exhibited a two-stage yielding. The first yielding is due to the induction of martensite upon loading rather than the rearrangement of martensite variants, because the Ti–26 at.% Nb alloy is β single phase at room temperature [14]. The critical stress for the first yielding and fracture strain did not change significantly. In contrast, the ultimate tensile strength (UTS) increased with increasing aging temperature reaching a maximum at 573 K; the UTS then decreased on further increasing the aging temperature to 873 K. The specimen heat treated at 873 K exhibited no age hardening, i.e. the UTS is the same as that of the solution-treated specimen.

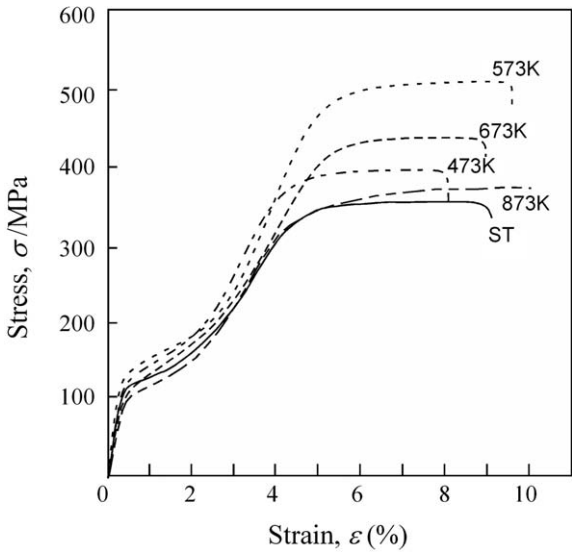

Fig. 7. Stress–strain curves of a solution-treated specimen (ST) and specimens aged at various temperatures between 473 and 873 K for 3.6 ks for the Ti–26 at.% Nb alloy.

Fig. 8(a) shows a dark-field TEM image and the corresponding selected-area diffraction pattern of the solution-treated Ti–26 at.% Nb alloy. The selected-area diffraction pattern was obtained from the $[1\,1\,0]_\beta$ zone axis. In addition to the primary reflections from the β matrix, diffuse scattering at 1/3 {1 1 2} positions corresponding to the athermal ω phase is visible in the selected-area diffraction pattern of the solution-treated specimen. A circle in the diffraction pattern indicates the spot of ω phase which was used to obtain the dark-field micrograph. A dispersion of very fine ω particles with a dimension of 3 nm was observed in the dark-field TEM image taken from the solution-treated specimen. The athermal ω phase in Ti–Nb binary alloys with compositions between 14 and 50 at.% Nb has been also observed in previous studies [15,19,22,23].

After aging at 473 K for 3.6 ks, the reflections from the ω phase became discrete spots and the size and volume fraction of the ω particles increased slightly as shown in the dark-field image if compared with the solution-treated specimen. With increasing aging temperature, the intensity of the ω diffraction spot increased. In the specimen aged at 573 K for 3.6 ks, the volume fraction of ω phase markedly increased, which is consistent with the strong ω reflections in the diffraction pattern. This indicates that the substantial increase of tensile strength after aging at 573 K is due to the growth of the thermal ω phase, instead of α phase. However, further increasing the aging temperature above 673 K resulted in a decrease of the volume fraction of ω phase. This is also consistent with the fact that the tensile strength decreased on further increasing the aging temperature from 673 to 873 K.

Fig. 9 shows the dark-field TEM images obtained from the specimens aged at 573 and 673 K for 36 ks. Aging at 573 K for 36 ks caused an increase in the size of the ω particles, as can be seen by comparing the ω particle size in Figs. 9(a) and 8(c). When the specimen was aged at 673 K for 36 ks, the coarsening of the ω particles can be seen more clearly. The average length of the ω particles increased up to 40 nm after aging at 673 K for 36 ks.

In order to investigate the orientation relationship between β phase and ω phase, a high-resolution TEM (HRTEM) study was carried out. Fig. 10(a) shows an example of a HRTEM image obtained from the specimen aged at 673 K for 36 ks. The incident beam was along the [1 1 0] direction of the β matrix. The corresponding fast Fourier transformation (FFT) diffraction pattern is also shown in Fig. 10(a). It is found that the FFT diffraction

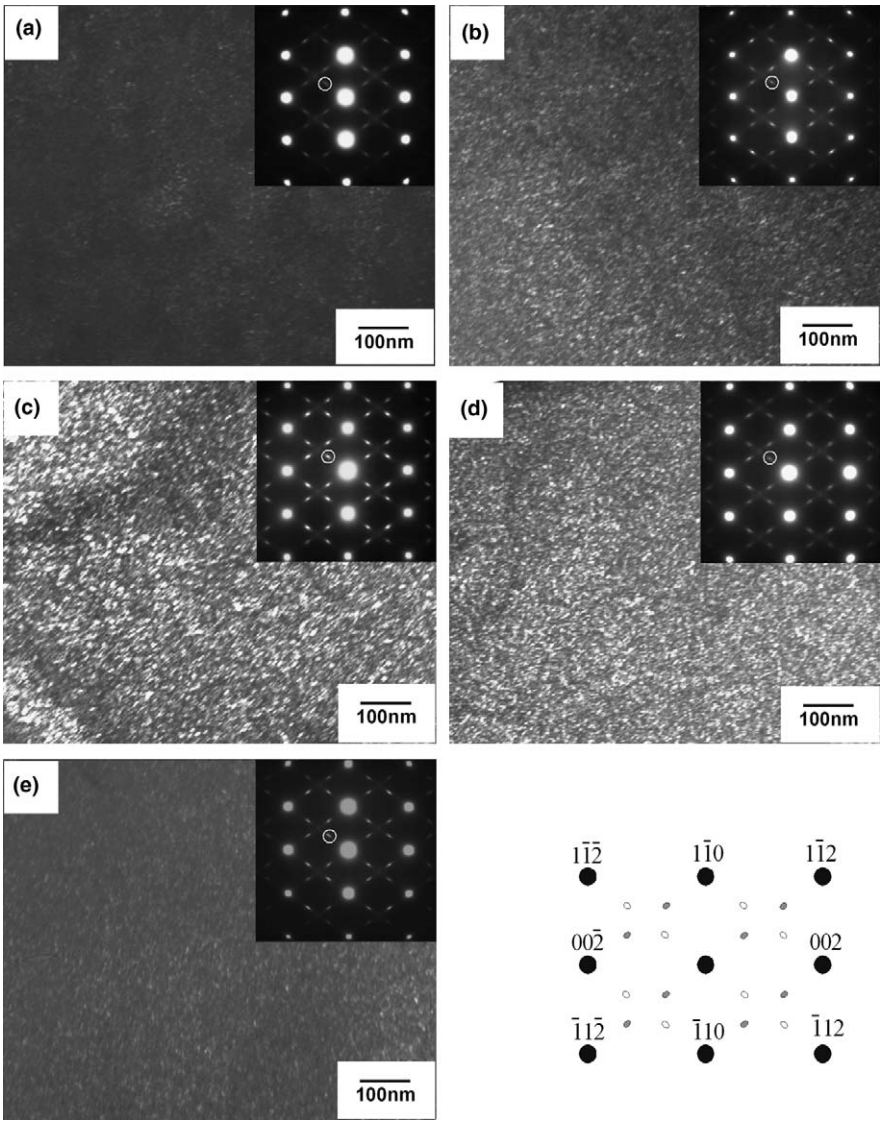

Fig. 8. Dark field TEM micrographs and the corresponding selected area diffraction patterns of (a) the solution treated Ti–26 at.% Nb alloy and specimens aged at (b) 473 K, (c) 573 K, (d) 673 K and (e) 873 K for 3.6 ks.

pattern is almost the same as the selected-area diffraction pattern shown in Fig. 9(b). Two different variants of ω phase can be seen in Fig. 10(a). It can be also seen that the ellipsoidal ω phase is elongated along one of the $\langle 1\,1\,1\rangle$ directions of the β phase. Fig. 10(b) shows a higher magnification HRTEM image. The lattice spacing of 0.23 nm corresponding to the $\{1\,1\,0\}$ planes of the β phase is visible at the upper part. The FFT diffraction pattern obtained from the ω phase in Fig. 10(b) indicates that the incident beam is parallel to $[\bar{1}\,2\,\bar{1}\,0]$ of the ω phase. The lattice spacings of 0.28 and 0.40 nm correspond to the $(0\,0\,0\,1)$ and $(1\,0\,\bar{1}\,0)$ planes of the ω phase, respectively. It is confirmed that the interface between the β phase and ω phase is coherent. It is seen that the ω phase has an orientation relationship with the β phase: $[0\,0\,0\,1]_{\omega}//[\bar{1}\,1\,1]_{\beta}$, $[1\,0\,\bar{1}\,1]_{\omega}//[1\,\bar{1}\,0]_{\beta}$ and $[\bar{1}\,2\,\bar{1}\,0]_{\omega}//[1\,1\,0]_{\beta}$. This is consistent with the well-established orientation relationship between ω and β, i.e. $\{0\,0\,0\,1\}_{\omega}//\{1\,1\,1\}_{\beta}$ and $[1\,1\,\bar{2}\,0]_{\omega}//[1\,\bar{1}\,0]_{\beta}$, in Ti- and Zr-based alloys. Fig. 10(b) also indicates the following relationship: $d_{(0\,0\,0\,1)\omega} = 3d_{(2\,2\,2)\beta} = \sqrt{3}a_{\beta}/2$. This confirms that the ω phase was formed by collapsing of two among three of the $\{1\,1\,1\}$ planes of the β phase into one plane at an intermediate position, retaining the third $(1\,1\,1)$ plane as a single layer, as suggested by de Fontaine [24].

3.3. Effect of isothermal ω phase on shape memory and superelastic behavior

In order to elucidate the effect of ω phase on shape memory and/or superelastic behavior, cyclic tensile tests were carried out at room temperature. Fig. 11 shows the stress–strain curves for a specimen subjected to solution treatment and specimens subjected to aging treatment at

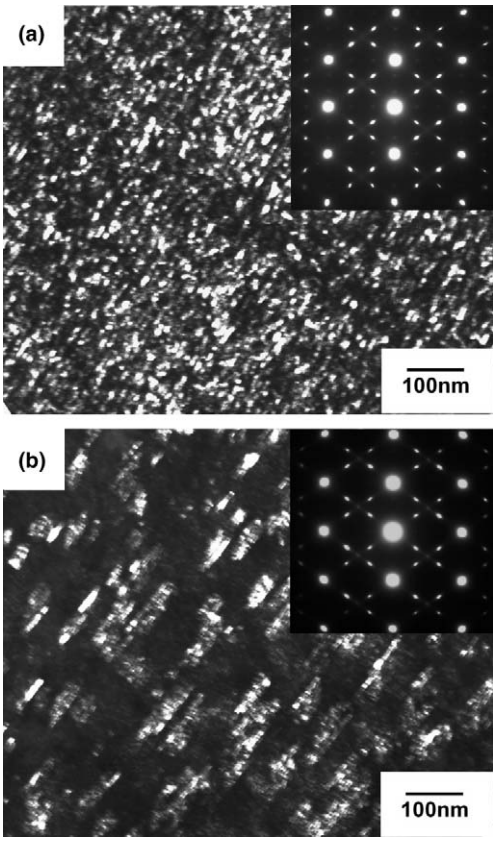

Fig. 9. Dark field TEM micrographs and the corresponding selected area diffraction patterns of the specimens aged at (a) 573 K and (b) 673 K for 36 ks.

673 K after the solution treatment. At the first cycle, tensile stress was applied until the strain reached about 1.5%, and then the stress was removed. The measurement was repeated by increasing the maximum strain by 0.5% upon loading for the same specimen. After unloading, the specimens that did not complete superelastic recovery were heated to about 500 K. The starting points of the stress–strain curves are shifted in order to separate each curve. Superelastic behavior was observed in the solution-treated specimen at the first cycle. With increasing tensile strain, the superelastic behavior became incomplete. The residual strains were almost completely recovered by heating at the second and third cycles. In order to characterize the shape memory behavior of the specimen, four types of strains are defined as follows: (1) the elastic strain ε_{el} recovered elastically upon unloading, (2) the recovered strain ε_{tr} due to the reverse transformation (which is equal to the sum of the transformation strain recovered superelastically upon unloading (ε_{se}) and the strain recovered by heating (ε_{sme})), (3) the total recovered strain ε_r consisting of ε_{el} and ε_{tr}, and (4) the permanently retained strain ε_p after unloading followed by the subsequent heating.

The magnitudes of ε_r and ε_{tr} are plotted as a function of tensile strain in Fig. 12(a). Almost perfect recovery was exhibited up to about 2.5% tensile strain for the solution-treated specimen. The data points deviate from the diagonal line beyond 2.5% strain. The residual permanent strain indicated by the deviation from the diagonal line increased with increasing tensile strain. ε_{tr} increased up to approximately 2.2% with increasing tensile strain. The specimen aged at 673 K for 3.6 ks exhibited almost perfect shape recovery up to about 4% tensile strain. It is important to note that the aged specimens revealed almost perfect superelasticity until the fourth cycle as shown in Fig. 11. When the specimen was unloaded after deforming up to 3% strain, only 0.3% of strain remained for both specimens aged at 673 K for 3.6 and 36 ks. The superelastically recovered strain increased up to about 3%, although ε_p increased with increasing cycle. The maximum ε_r of 4.2% and maximum ε_{tr} of 2.8% were obtained for the specimen aged at 673 K for 3.6 ks as can be seen in Fig. 12. It is noted that the maximum ε_{tr} of 2.8% obtained by the cyclic tensile test for the Ti–26 at.% Nb aged at 673 K for 3.6 ks is quite close to the transformation strain along [0 1 1] estimated from Eq. (3). It is supposed that this is due to the recrystallization texture developed during the solution treatment. It has been reported that a strong recrystallization texture of $\{1\,1\,2\}\ \langle 1\,\bar{1}\,0\rangle$ is developed in β-Ti-based alloys such as Ti–22Nb–6Ta [25] and Ti–22Nb–3Al [26] solution treated in the temperature range between 1173 and 1273 K after severe cold-rolling.

For the specimen aged for 36 ks, it is obvious that the critical stress for the first yielding increased when compared with the solution-treated specimen. This means that the stress for inducing martensite increased with an increasing amount of ω phase, and this resulted in a decrease in the maximum recovered strain of the specimen aged at 673 K for 36 ks. It is well known that the ω phase is Ti-rich [27], although the exact composition of ω phase is difficult to determine. This implies that the increase in the amount of ω phase increases the Nb content of the matrix, resulting in a decrease of the martensitic transformation temperature. The dispersed ω particles mechanically suppress the martensitic transformation, also causing the transformation temperature to decrease. As a result, it is reasonable that the stress for inducing martensite increased with an increasing amount of ω phase. Stable superelasticity was observed even though the maximum stress reached 460 MPa upon loading in the specimen.

The total recovered strain and retained plastic strain are plotted as a function of applied stress in Fig. 12(b). In general, the stability of shape memory and superelastic behavior is evaluated by the critical stress for slip deformation (σ_s). This is defined as a stress inducing 0.5% plastic strain in this study. σ_s was determined as 400 MPa for the solution-treated specimen. σ_s increased with increasing aging time. For the specimen aged at 673 K for 36 ks, σ_s reached 550 MPa, which resulted in stable superelasticity. This suggests that the stable superelasticity and larger recovery strain were due to the decrease in the transformation temperatures and the increase in the critical stress for plastic deformation in the aged specimens.

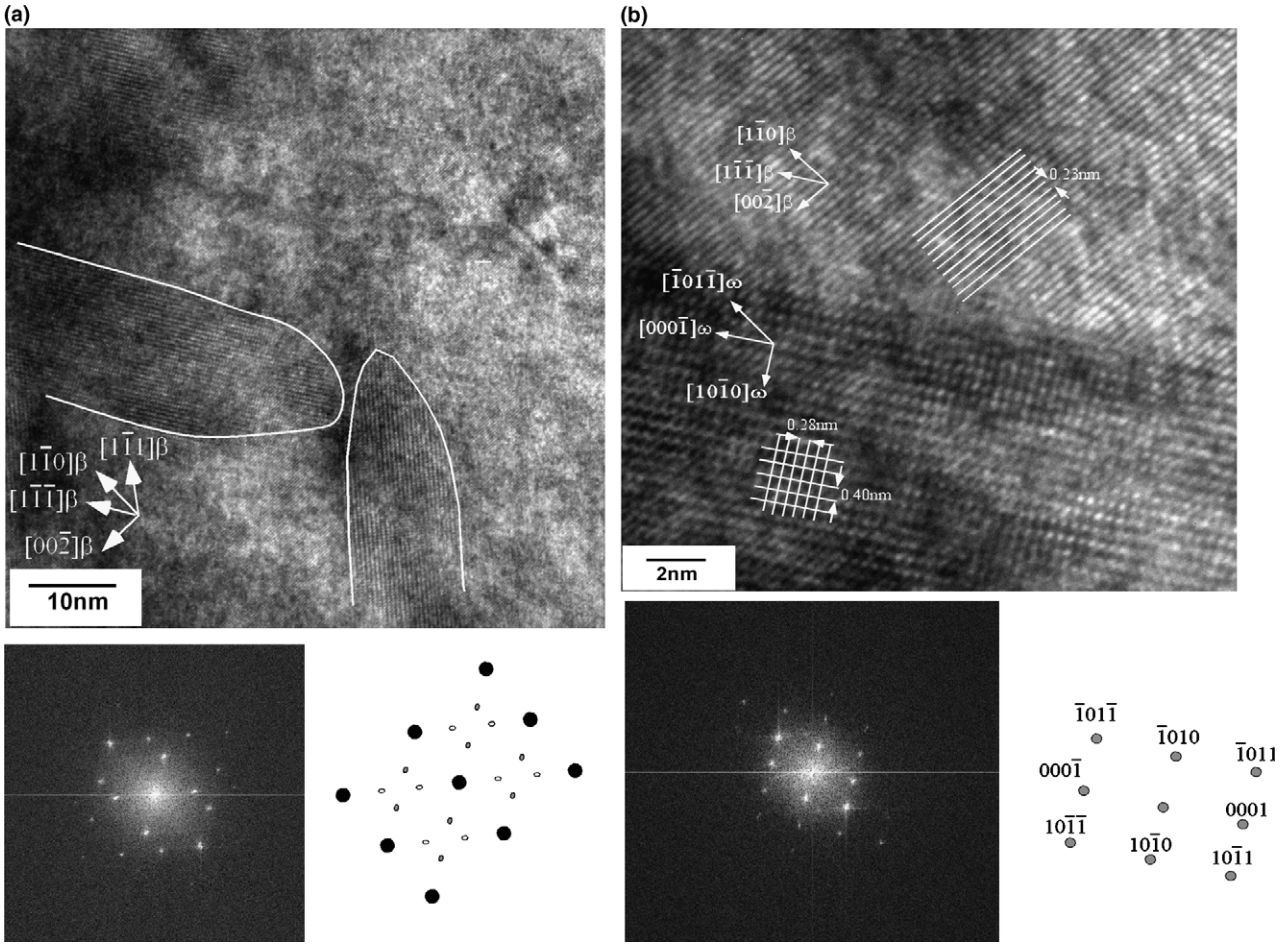

Fig. 10. (a) A high resolution TEM micrograph and the corresponding FFT diffraction pattern obtained from the specimen aged at 673 K for 36 ks; (b) a higher magnification HRTEM micrograph and the corresponding FFT diffraction pattern.

Fig. 13 shows the stress–strain curves obtained by strain increment cyclic tensile tests for the specimens subjected to aging treatment at 573 K. The specimen aged at 573 K for 3.6 ks exhibited almost perfect superelasticity at the first and second cycles. The superelastically recovered strain increased with increasing applied strain although the retained plastic strain increased. For the specimen aged at 573 K for 36 ks, it is obvious that the critical stress for the first yielding, which corresponds to the stress for inducing martensite, increased and the superelasticity was stabilized when compared with the specimen aged at 573 K for 3.6 ks. The maximum superelastic strain of 2.9% was obtained by aging at 573 K for 36 ks. It is also noted that stable superelasticity was observed even though the maximum stress reached 520 MPa upon loading in the specimen. The critical stress for the first yielding and the maximum stress reached at each cycle are higher when compared with the specimen aged at 673 K for 36 ks as can be seen by comparing with the results in Fig. 11. This seems reasonable because the high-density fine ω precipitates are more effective for increasing the stresses inducing the martensitic transformation and plastic deformation. This can easily be confirmed by the TEM images in Fig. 9. The ω phase precipitated with a very high density with a size of about 15 nm in the specimen aged at 573 K for 36 ks. In contrast, when the aging is conducted at 673 K for 36 ks, the precipitates are larger and the density is lower. It has also been reported by Kim and Miyazaki [28] that fine and dense Ti_3Ni_4 precipitates (<10 nm) act as effective obstacles such as pinning points against the movement of dislocations in Ni-rich Ti–Ni alloys. They also suggested that the shape memory behavior of Ni-rich Ti–Ni alloys can be improved by increasing the density of nanoscaled Ti_3Ni_4 precipitates which are formed by aging at low temperatures ranging between 473 and 573 K. It is generally accepted that the ω phase results in high hardness and brittleness; thus the aging treatment for precipitation of the ω phase is avoided in Ti-based alloys. However, in this study, it is suggested that the fine ω precipitates are effective in improving the shape memory and superelastic properties by increasing the critical stress for plastic deformation.

3.4. Effect of annealing temperature on shape memory and superelastic behavior

In order to investigate the effect of annealing conditions on shape memory and superelastic behavior, strain incre-

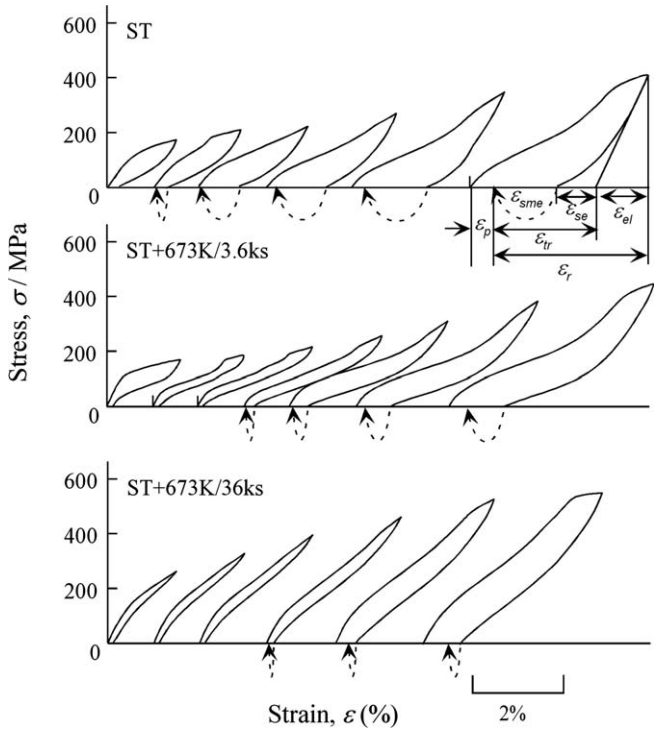

Fig. 11. Stress–strain curves obtained from cyclic loading–unloading tensile tests for the solution treated specimen and the specimens aged at 673 K for 3.6 and 36 ks.

ment cyclic tensile tests were carried out for the specimen subjected to annealing at 873 K for 0.6 ks (ITA, intermediate-temperature annealing), and the result is shown in Fig. 14. Fig. 14 also shows the stress–strain curves for the specimen annealed at 873 K for 0.6 ks followed by aging treatment at 573 K for 3.6 ks (ITA + AG). Perfect superelasticity was obtained at the first cycle in the ITA specimen. It can be seen that the tensile stress at each cycle is higher and the stress hysteresis is smaller when compared with the results for the solution-treated specimen shown in Fig. 11. Fig. 15(a) shows a bright-field TEM image revealing a recovered microstructure with fine subgrains consisting of a high density of thermally rearranged dislocations in the specimen annealed at 873 K. It is noted that fine ω particles with a dimension of 3 nm were also observed in the dark-field TEM image (Fig. 15(b)). This suggests that fine subgrains and a high density of thermally rearranged dislocations stabilized the superelasticity for the specimen heat treated at 873 K. Furthermore, it can be seen that the ITA + AG specimen exhibited excellent superelasticity. Perfect superelasticity was observed until the fourth cycle. Superelastic behavior can be obtained even though the maximum stress reached 660 MPa upon loading in the ITA + AG specimen. It is also noted that the ITA + AG specimen exhibited more stable superelasticity when compared with the solution-treated + AG specimen shown in Fig. 13, due to the combined effect of work hardening and age hardening.

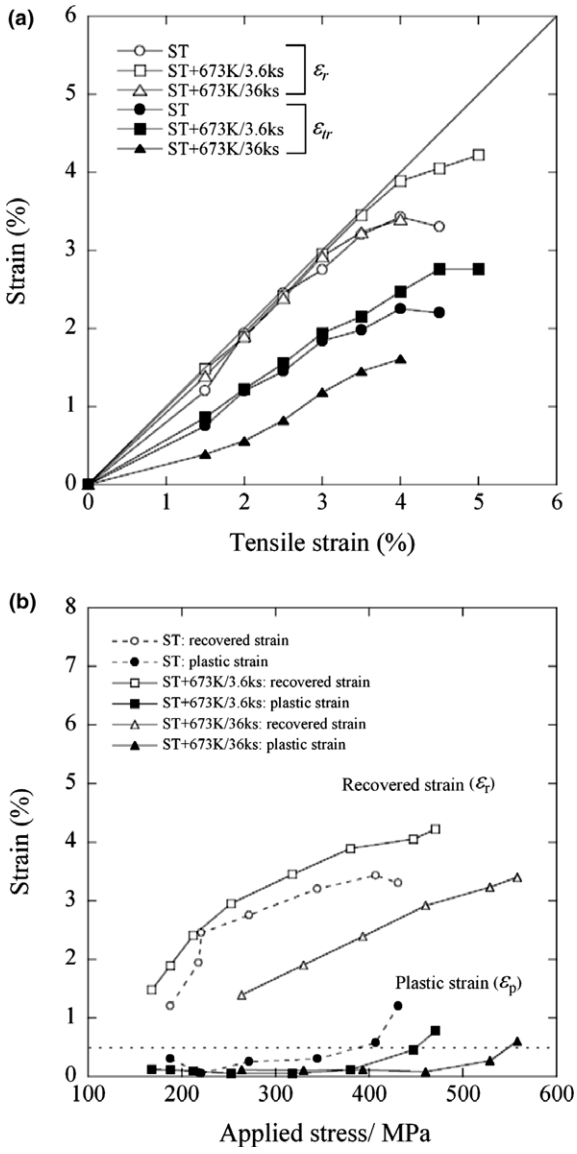

Fig. 12. Total recovered strain (ε_r), transformation strain (ε_{tr}) and plastic strain (ε_p) obtained by cyclic loading–unloading tensile tests as shown in Fig. 11. (a) ε_r and ε_{tr} as a function of tensile strain; (b) ε_r and ε_p as a function of maximum applied stress of each cycle.

The magnitudes of the retained plastic strain and the superelastic strain including elastic strain were measured at each cycle in Fig. 14, and they are plotted as a function of applied stress at each cycle in Fig. 16. The data for the solution-treated specimen are also plotted for comparison. It can be seen that σ_s of the solution-treated specimen increased from 400 to 490 MPa on aging at 573 K for 3.6 ks. It can be seen that the ITA specimen revealed a higher σ_s when compared with the solution-treated specimen. σ_s of the ITA specimen further increased on aging at 573 K for 3.6 ks, which resulted in a larger superelastic strain for the ITA + AG specimen. Fig. 16 reveals that the maximum superelastic strain of 3.3% was obtained in the ITA + AG specimen.

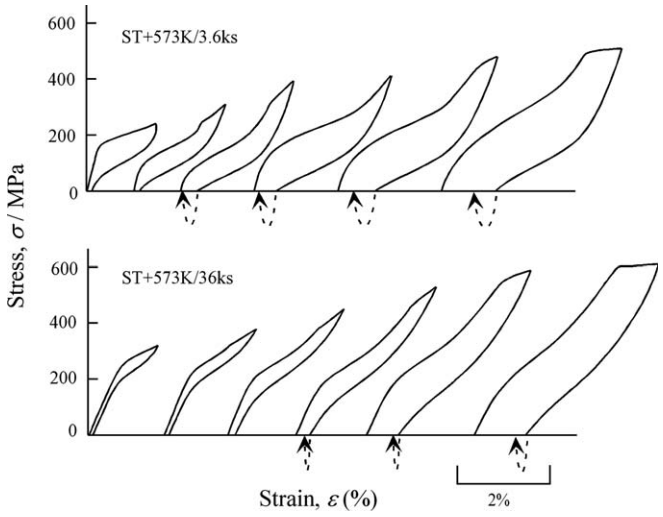

Fig. 13. Stress–strain curves obtained by cyclic loading–unloading tensile tests for the specimens aged at 573 K for 3.6 and 36 ks.

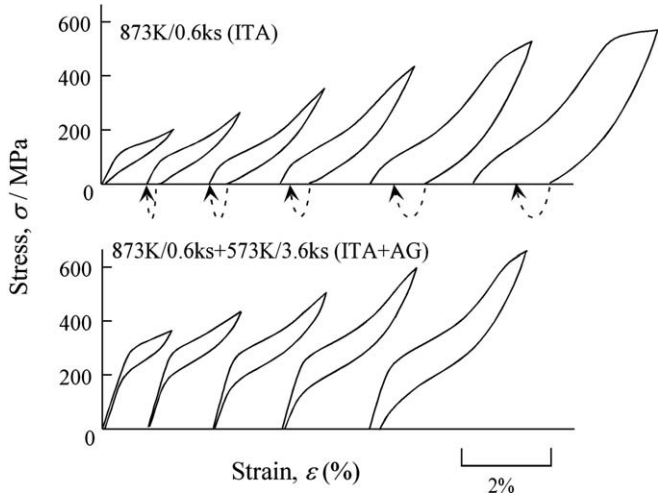

Fig. 14. Stress–strain curves obtained by cyclic loading–unloading tensile tests for the specimen annealed at 873 K for 0.6 ks (ITA) and the specimen aged at 573 K for 3.6 ks after annealing treatment (ITA + AG).

In order to investigate the stability of the superelasticity of the ITA + AG specimen, a cyclic tensile test was carried out by elongating the tensile specimen up to 2.5% strain followed by unloading. The results are shown in Fig. 17. The ITA + AG specimen exhibited almost perfect superelastic behavior from the first cycle. The apparent yield stress indicated by an arrow, which is the stress for inducing the martensitic transformation, decreased slightly with increasing cycle number up to the third cycle. However, it was constant after the third cycle irrespective of increasing cycle number. This is same tendency observed in Ti–Ni alloys during cyclic deformation. It has been reported that the critical stress to induce the martensitic transformation decreases with increasing cyclic deformation in Ti–Ni alloys, since the internal stress field formed by the accumulation of dislocations introduced during cyclic loading assists the formation of the stress-induced martensites

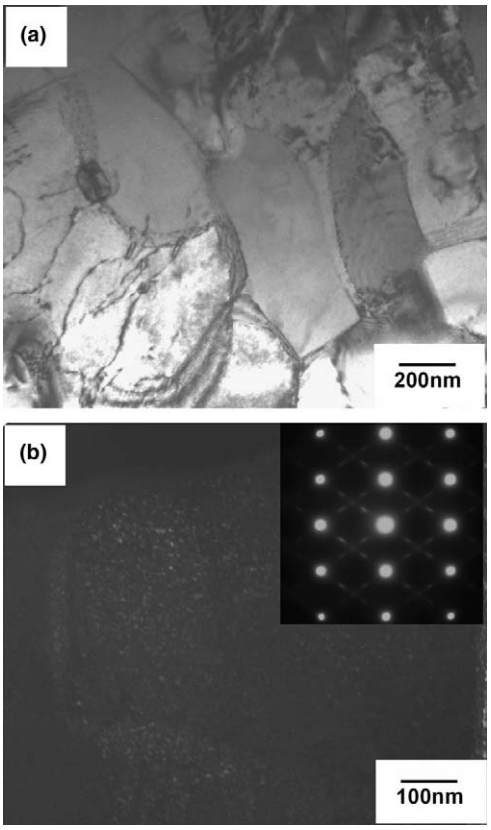

Fig. 15. (a) A bright-field TEM micrograph and (b) a dark field TEM micrograph with the corresponding selected area diffraction pattern of the specimen annealed at 873 K for 0.6 ks.

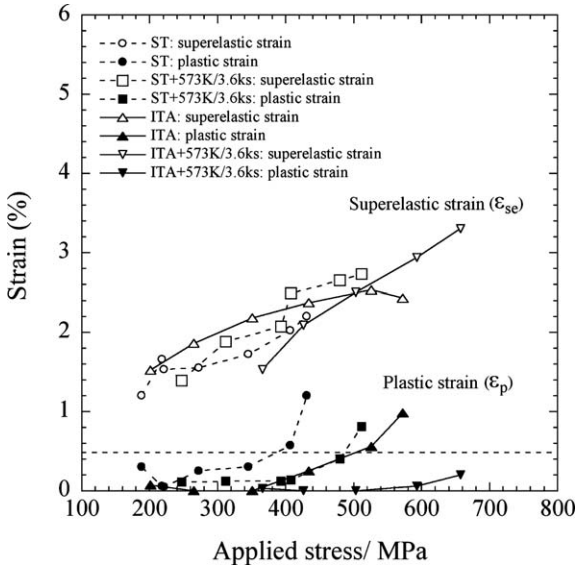

Fig. 16. The superelastic strain and the remained plastic strain as a function of applied stress for the ST, ST + AG, ITA and ITA + AG specimens.

[29]. After the second cycle, complete superelastic behavior is observed with a narrow stress hysteresis. As a result, it can be concluded that excellent superelasticity can be

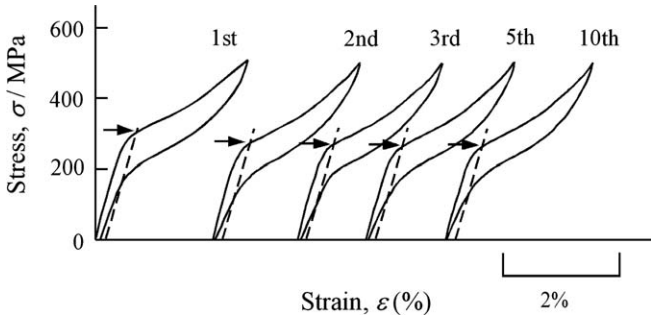

Fig. 17. Stress–strain curves obtained by cyclic tensile tests by elongating a tensile specimen up to 2.5% strain followed by unloading for each cycle in the ITA + AG specimen.

achieved by annealing at an intermediate temperature lower than the recrystallization temperature followed by aging at a lower temperature in binary Ti–Nb alloys.

4. Conclusions

(1) Transformation strains were calculated using the lattice constants and the lattice correspondence between the β and α″ phases. The maximum transformation strain was obtained along the [0 1 1] direction of the β phase. The transformation strain linearly decreased with increasing Nb content.

(2) Athermal ω particles with a dimension of 3 nm were observed in the solution-treated Ti–26 at.% Nb alloy. The size and volume fraction of the ω phase increased with increasing aging temperature from 473 to 573 K. However, further increasing the aging temperature above 673 K resulted in a decrease of the size and volume fraction of the ω phase. The average length of the ω phase increased to 15 and 40 nm after aging at 573 and 673 K for 36 ks, respectively.

(3) The ω phase coarsened while maintaining an orientation relationship with the β phase during aging at temperatures between 473 and 673 K: $\{0\,0\,0\,1\}_\omega // \{1\,1\,1\}_\beta$ and $[1\,1\,\bar{2}\,0]_\omega // [1\,\bar{1}\,0]_\beta$. The ω phase is of ellipsoidal shape elongated along each of the ⟨1 1 1⟩ directions of the β phase which is parallel to the [0 0 0 1] direction of the ω variant.

(4) The critical stress for slip increased with increasing size and volume fraction of the ω precipitates. A higher critical stress for slip resulted in a larger recovery strain and stable superelasticity in the specimens aged at 673 K. The maximum recovered strain of 4.2% was obtained for the specimen aged at 673 K for 3.6 ks. The high density of fine precipitates for the specimen aged at 573 K for 3.6 ks is more effective in increasing the stress for inducing the martensitic transformation and the critical stress for plastic deformation, resulting in good superelasticity.

(5) The intermediate-temperature annealing at 873 K for 0.6 ks formed fine subgrains and a high density of thermally rearranged dislocations which resulted in a higher critical stress for permanent deformation. Excellent superelasticity with a recoverable strain of 3.3% can be obtained even though the maximum stress reached 660 MPa on intermediate-temperature annealing followed by aging at 573 K.

Acknowledgment

This work was supported in part by the 21 Century Center of Excellence Program and the Grants-in-Aid for Fundamental Scientific Research (Kiban A(1999–2001), Kiban A(2002–2004)) from the Ministry of Education, Culture, Sports, Science and Technology, Japan.

References

[1] Duerig TW, Albrecht J, Richter D, Fischer P. Acta Metall 1982;30:2161–72.
[2] Grosdidier T, Philippe MJ. Mater Sci Eng A 2000;291:218–23.
[3] Takahashi E, Sakurai T, Watanabe S, Masahashi N, Hanada S. Mater Trans 2002;43:2978–83.
[4] Maeshima T, Nishida M. Mater Trans 2004;45:1096–100.
[5] Zhou T, Aindow M, Alpay SP, Blackburn MJ, Wu MH. Scripta Mater 2004;50:343–8.
[6] Fukui Y, Inamura T, Hosoda H, Wakashima K, Miyazaki S. Mater Trans 2004;45:1077–82.
[7] Kim HY, Ohmatsu Y, Kim JI, Hosoda H, Miyazaki S. Mater Trans 2004;45:1090–5.
[8] Baker C. Metal Sci J 1971;5:92–100.
[9] Lei CY, Pak JSL, Inoue HRP, Wayman CM. In: Proceedings of the international conference on martensitic transformations. Monterey, CA: Monterey Institute for Advanced Studies; 1992. p. 539.
[10] Sasano H, Suzuki T. In: Proceedings of the fifth international conference on titanium. Frankfurt, Germany: Deutsche Gesellschaft fur Metallkunde; 1985. p. 1667.
[11] Kim JI, Kim HY, Inamura T, Hosoda H, Miyazaki S. Mater Sci Eng A 2005;403:334–9.
[12] Kim JI, Kim HY, Hosoda H, Miyazaki S. Mater Trans 2005;46:852–7.
[13] Kim HY, Hashimoto S, Kim JI, Inamura T, Hosoda H, Miyazaki S. Mater Sci Eng A 2006;417:120–8.
[14] Kim HY, Satoru H, Kim JI, Hosoda H, Miyazaki S. Mater Trans 2004;45:2443–8.
[15] Moffat DL, Larbalestier DC. Metall Trans A 1988;19A:1677–86.
[16] Morniroli JP, Gantois. Mem Sci Rev Metall 1973;70:831–42.
[17] Baker C, Sutton J. Philos Mag 1969;19:1223–55.
[18] Jepson KS, Brown ARG, Gray JA. The science, technology and application of titanium. Pergamon Press; 1970. p. 677.
[19] Ahmed T, Rack HJ. J Mater Sci 1996;31:4267–76.
[20] Matsumoto H, Watanabe S, Hanada S. Mater Trans 2005;46:1070–8.
[21] Brown ARG, Clark D, Eastabrook J, Jepson KS. Nature 1964;201:914–5.
[22] Balcerzak AT, Sass SL. Metall Trans 1972;3:1601–5.
[23] Hanada S, Izumi O. Metall Trans A 1986;17A:1409–20.
[24] deFontaine D. Acta Metall 1970;18:275–9.
[25] Kim HY, Sasaki T, Okutsu K, Kim JI, Inamura T, Hosoda H, et al. Acta Mater 2006;54:423–33.
[26] Inamura T, Fukui Y, Hosoda H, Wakashima K, Miyazaki S. Mater Trans 2004;45:1083–9.
[27] Williams JC. In: Proceedings of the second international conference on titanium. New York, NY: Plenum Press; 1973. p. 1433.
[28] Kim JI, Miyazaki S. Acta Mater 2005;53:4545–54.
[29] Miyazaki S, Imai T, Igo Y, Otsuka K. Metall Trans A 1986;17A:115–20.